Available online at www.sciencedirect.com
ScienceDirect
Journal of Magnetic Resonance 188 (2007) 344–356
JMR Journal of Magnetic Resonance
www.elsevier.com/locate/jmr

# Lineshapes and artifacts in Multidimensional Fourier Transform of arbitrary sampled NMR data sets

Krzysztof Kazimierczuk [a], Anna Zawadzka [a], Wiktor Koźmiński [a,*], Igor Zhukov [b,c]

[a] Department of Chemistry, Warsaw University, ul. Pasteura 1, 02-093 Warszawa, Poland
[b] Institute of Biochemistry and Biophysics, Polish Academy of Sciences, ul. Pawińskiego 5a, 02-106 Warszawa, Poland
[c] Slovenian NMR Centre, National Institute of Chemistry, Hajdrihova 19, SI-1001 Ljubljana, Slovenia

Received 11 June 2007; revised 7 August 2007
Available online 15 August 2007

**Abstract**

The comprehensive description of Multidimensional Fourier Transform applied to arbitrary sampled NMR data is presented. Lineshapes and signal-to-artifact ratio are discussed in detail with regard to time domain sampling scheme and applied data weighting. It is demonstrated that transformation method with simple summation instead of numerical integration is most useful for significantly undersampled experiments. Additionally, the optimized random sampling schedule which enables significant improvement of obtained spectra is proposed. The new procedure of cleaning spectra is presented, it is based on predictability of artifacts pattern when sampling scheme and amplitude of intense signals are known. The results enable observation of high dynamic range spectra as for example heteronuclear edited NOESY. We show the application of new approach to the 3D $^{15}$N-edited NOESY-HSQC spectrum acquired for $^{13}$C, $^{15}$N labeled ubiquitin sample with random time domain sampling.


*Keywords:* NMR spectroscopy; Multidimensional Fourier Transform; Data sampling; Sparse sampling; Proteins; Fast multidimensional data acquisition; NOESY; Hypercomplex numbers

## 1. Introduction

The key advantage of multidimensional NMR spectroscopy [1] is resolving of spectral frequencies by spanning them in different dimensions. Therefore, it enables one to assign individual correlation peaks to group of mutually interacting nuclei, and thus provides unique source of information about biomolecular structure, interactions, and dynamics. However, despite of gradually increasing sensitivity of modern NMR spectrometers, the main limitation of multidimensional NMR experiments is measurement time which grows rapidly with number of dimensions and expected resolution. This is because of Nyquist theorem sampling requirements (Eq. (1)) for conventional acquisition with data points lying on the Cartesian grid.

$$\Delta t_i \leqslant (\mathrm{sw}_i)^{-1} \tag{1}$$

where $\Delta t_i$ is delay between time points in $i$-time domain, and $\mathrm{sw}_i$ is required spectral width. While the resolution increases with sampling of longer resolution time, using of $\Delta t_i$ above Nyquist limit results in ambiguity of frequency discrimination commonly referred as signal folding. The natural limitation of maximum evolution time by signal decay due to transverse relaxation is, in the most cases, not reachable in ND NMR spectroscopy ($N > 2$) even for biomolecules outside of extreme narrowing regime. In the all cases conventional processing of multidimensional NMR spectra employs sequential application of 1D discrete complex Fourier Transform (Eq. (2)) in consecutive time domains.

* Corresponding author. Fax: +48 22 822 59 96.
*E-mail address:* kozmin@chem.uw.edu.pl (W. Koźmiński).

1090-7807/$ - see front matter © 2007 Elsevier Inc. All rights reserved.
doi:10.1016/j.jmr.2007.08.005

$$S(\omega) = \sum_{t=0}^{t_{\max}} f(t) \exp(-\mathrm{i}\omega t) \tag{2}$$

Therefore, for example 2D FT, applied to signal $f(t_1, t_2)$, could be described for convenience as in Eqs. (3ab), with the spectrum computed in the two separate steps:

$$f(t_1, t_2) \overset{\mathrm{FT}_2}{\rightarrow} g(t_1, \omega_2) \overset{\mathrm{FT}_1}{\rightarrow} S(\omega_1, \omega_2)$$

In the first, all summations with respect of $t_2$ are calculated and give rise to mixed time/frequency domain signal $g(t_1, \omega_2)$, followed by series of summation with respect to $t_1$, in the second step, resulting in spectrum $S(\omega_1, \omega_2)$:

$$g(t_1, \omega_2) = \sum_{t_2=0}^{t_{2\max}} f(t_1, t_2) \exp(-\mathrm{i}\omega_2 t_2) \tag{3a}$$

$$S(\omega_1, \omega_2) = \sum_{t_1=0}^{t_{1\max}} g(t_1, \omega_2) \exp(-\mathrm{i}\omega_1 t_1) \tag{3b}$$

In recent years several new approaches for non-conventional probing of evolution time space were developed and allowed for an acceleration of multidimensional experiments.

The idea of Accordion Spectroscopy [2,3] was employed in radial sampling followed by radial 1D FT with multiple quadrature. It enabled direct evaluating of frequencies from projection spectra by solving systems of linear equations for each peak in the new variants of Reduced Dimensionality (RD) techniques [4–6]. The same kind of sampling of time domain, but along set of radial directions, allows also for calculation of full dimensionality spectra employing methods based on backprojection [7] imaging technique using different strategies [8–16]. Other methods of fast acquisition include: multidimensional decomposition [17–19], filter diagonalization [20,21], maximum entropy reconstruction [22–26], and spatially encoded chemical shift evolution followed by spatially resolved acquisition [27]. Also, algorithms of Fast Fourier Transform (FFT) of non-equispaced data based on polynomial interpolation [28] were employed to reconstruct spectrum from sparsely sampled data sets [29].

Recently, we have shown [30–32] that the application of FT with respect to two or more time variables simultaneously is a reliable approach to processing of arbitrary sampled multidimensional NMR data sets. In this method, referred below as Multidimensional Fourier Transform (MFT), contrary to conventional 2D FT computed sequentially using Eq. (3), computation of point of 2D spectrum $S(\omega_1, \omega_2)$ is performed in a single step according to Eq. (4), where $w(t_1, t_2)$ denotes discussed later weights:

$$S(\omega_1, \omega_2) = \sum_{t_1=0}^{t_{1\max}} \sum_{t_2=0}^{t_{2\max}} \exp(-\mathrm{i}\omega_1 t_1) f(t_1, t_2) \exp(-\mathrm{j}\omega_2 t_2) w(t_1, t_2)$$
$$\mathrm{i}^2 = \mathrm{j}^2 = \mathrm{k}^2 = -1 \quad \text{and} \quad \mathrm{ij} = \mathrm{ji} = \mathrm{k},$$
$$\mathrm{jk} = \mathrm{kj} = -\mathrm{i}, \ \mathrm{ki} = \mathrm{ik} = -\mathrm{j} \tag{4}$$

MFT as given in Eq. (4) does not require data points distributed in rows and columns contrary to conventional approach employing sequence of 1D transforms. Therefore, the key feature of MFT is its ability to obtain spectrum using arbitrary sampling pattern in the time domain. In such case it is generally not possible to employ FFT algorithms. We have shown examples using radial, spiral sampling [30], and we have found that best results can be achieved employing random time domain points distribution [31]. Additionally, in the later case of irregular sampling no signal folding is observed. These results were confirmed by other groups for radial [33,34], concentric rings [35], and recently for random sampling [36]. The 2D MFT as defined in Eq. (4) provides identical results as conventional when evolution time domain is sampled using Cartesian grid.

The significant drawback of MFT applied to sparsely sampled interferograms are artifacts appearing due to ambiguities and irregular data points distribution. The simplest artifacts pattern is observed for radial sampling. It forms tilted lines crossing at the signal position, its origin are ambiguities identical as obtained in backprojection techniques. In the case of spiral sampling the artifact pattern is more dispersed but still dependent on actual sampling parameters. The lowest level of artifacts is observed for random sampling. The signal-to-artifact ratio increases with square root of number of data points, exactly like in the case of always present thermal noise.

In all cases, the artifact pattern is determined by time domain points distribution. In this paper we analyze origin and pattern of artifacts in relation to sampling scheme and applied processing. We show that sampling artifacts can be significantly reduced by coarse determination of strong peaks frequencies, prediction of the form and amplitude of sampling noise followed by artifact subtraction. This procedure is especially valuable for spectra with high dynamic range of peak amplitudes as for example NOESY.

## 2. Theory

### 2.1. Multidimensional FT

The 2D case of MFT is given in Eq. (4). It should be pointed out that, as an extension of complex 1D FT, ND case of MFT requires hypercomplex notation to properly describe quadrature. In the general $N$-dimensional case MFT quadrature could be shortly described using commutative Clifford Fourier Transform [37–39].

In practice, numerical computations are performed on real numbers, thus the real part of discrete 1D FT (Eq. (2)) should be evaluated, assuming signal $f(t) = \exp(\mathrm{i}\Omega t)$ as

$$\mathrm{Re}[S(\omega)] = \sum_{t=0}^{t_{\max}} \cos(\Omega t)\cos(\omega t) + \sum_{t=0}^{t_{\max}} \sin(\Omega t)\sin(\omega t) \tag{5}$$

Independently of processing method to obtain full information about signs of frequencies in 2D experiment one

needs to acquire separately four different modulations (Eqs. (6a)–(6d)), where $\Omega$ is signal frequency:

$$f(t_1,t_2)=\cos(\Omega_1 t_1)\cos(\Omega_2 t_2) \tag{6a}$$
$$f'(t_1,t_2)=\cos(\Omega_1 t_1)\sin(\Omega_2 t_2) \tag{6b}$$
$$f''(t_1,t_2)=\sin(\Omega_1 t_1)\cos(\Omega_2 t_2) \tag{6c}$$
$$f'''(t_1,t_2)=\sin(\Omega_1 t_1)\sin(\Omega_2 t_2) \tag{6d}$$

In the conventional 2D FT approach Eqs. (6a) with (6b) represent real, and (6c) with (6d) imaginary parts of signal in $t_1$, i.e., $\cos(\Omega_1 t_1)\exp(\mathrm{i}\Omega_2 t_2)$ and $\sin(\Omega_1 t_1)\exp(\mathrm{i}\Omega_2 t_2)$, respectively. Whereas, (6a) with (6c) and (6b) with (6d) are real and imaginary components of signal in $t_2$: $\exp(\mathrm{i}\Omega_1 t_1)\cos(\Omega_2 t_2)$ and $\exp(\mathrm{i}\Omega_1 t_1)\sin(\Omega_2 t_2)$. The complex vectors (Eqs. (6ab) and (6cd)) are transformed separately with respect to $t_2$, resulting in the complex interferogram $g(t_1,\omega_2)$ (Eqs. (7ab)) which is used for subsequent 1D FT in $t_1$.

$$g(t_1,\omega_2)=\mathrm{Re}[S(t_1,\omega_2)]\exp(\mathrm{i}\Omega_1 t_1) \tag{7a}$$
$$g'(t_1,\omega_2)=\mathrm{Im}[S(t_1,\omega_2)]\exp(\mathrm{i}\Omega_1 t_1) \tag{7b}$$

In the case of 2D MFT the simplest way is to treat signal $f(t_1,t_2)$ defined in Eqs. (6a)–(6d) as the hypercomplex number:

$$\begin{aligned} f(t_1,t_2) &= \cos(\Omega_1 t_1)\cos(\Omega_2 t_2)+\mathrm{i}\sin(\Omega_1 t_1)\cos(\Omega_2 t_2)\\ &\quad +\mathrm{j}\cos(\Omega_1 t_1)\sin(\Omega_2 t_2)+\mathrm{k}\sin(\Omega_1 t_1)\\ &\quad \times \sin(\Omega_2 t_2)\\ &= \exp(\mathrm{i}\Omega_1 t_1)\exp(\mathrm{j}\Omega_2 t_2) \end{aligned} \tag{8}$$

Therefore, the real part of 2D MFT as defined in Eq. (4), can be described as a sum of four terms given in Eq. (9):

$$\begin{aligned} &\mathrm{Re}[S(\omega_1,\omega_2)]\\ &= \sum_{t_1=0}^{t_{1\max}}\sum_{t_2=0}^{t_{2\max}}\cos(\Omega_1 t_1)\cos(\Omega_2 t_2)\cos(\omega_1 t_1)\cos(\omega_2 t_2)\\ &\quad +\sum_{t_1=0}^{t_{1\max}}\sum_{t_2=0}^{t_{2\max}}\sin(\Omega_1 t_1)\cos(\Omega_2 t_2)\sin(\omega_1 t_1)\cos(\omega_2 t_2)\\ &\quad +\sum_{t_1=0}^{t_{1\max}}\sum_{t_2=0}^{t_{2\max}}\cos(\Omega_1 t_1)\sin(\Omega_2 t_2)\cos(\omega_1 t_1)\sin(\omega_2 t_2)\\ &\quad +\sum_{t_1=0}^{t_{1\max}}\sum_{t_2=0}^{t_{2\max}}\sin(\Omega_1 t_1)\sin(\Omega_2 t_2)\sin(\omega_1 t_1)\sin(\omega_2 t_2) \end{aligned} \tag{9}$$

It should be noted that basis functions of hypercomplex 2D Fourier Transform differ from basis functions of 2D complex Fourier Transform [40].

In order to use interactive phasing of resulted spectra it would be necessary to calculate not only the real part of MFT given in Eq. (9), but also additionally three imaginary parts of Eq. (4). However, due to saving of computing time, it is always preferable to set pulse sequence to obtain correct and predictable zero and first order phases in indirectly sampled time domains, and include time domain phases in Eq. (9).

## 3. Results

### 3.1. Conventional sampling and MFT

In the case of conventional sampling, the result of one-step MFT procedure is equal to that obtained by sequence of 1D transforms. Proof of this fact is quite simple:

$$\begin{aligned} S(\omega_1,\omega_2) &= \mathrm{FT}_1\{\mathrm{FT}_2[f(t_1,t_2)]\}\\ &= \sum_m\left(\sum_n f(t_1^m,t_2^n)\exp(-\mathrm{i}\omega_2 t_2^n)\right)\exp(-\mathrm{j}\omega_1 t_1^m)\\ &= \sum_m\left[f(t_1^m,t_2^1)\exp(-\mathrm{i}\omega_2 t_2^1)+f(t_1^m,t_2^2)\exp(-\mathrm{i}\omega_2 t_2^2)\right.\\ &\quad \left.+\cdots+f(t_1^m,t_2^N)\exp(-\mathrm{i}\omega_2 t_2^N)\right]\exp(-\mathrm{j}\omega_1 t_1^m)\\ &= \left[f(t_1^m,t_2^1)\exp(-\mathrm{i}\omega_2 t_2^1)+f(t_1^m,t_2^2)\exp(-\mathrm{i}\omega_2 t_2^2)\right.\\ &\quad \left.+\cdots+f(t_1^m,t_2^N)\exp(-\mathrm{i}\omega_2 t_2^N)\right]\\ &\quad \times\left[\exp(-\mathrm{j}\omega_1 t_1^1)+\cdots+\exp(-\mathrm{j}\omega_1 t_1^M)\right]\\ &= \sum_{m,n} f(t_1^m,t_2^n)\exp(-\mathrm{i}\omega_1 t_1^m)\exp(-\mathrm{j}\omega_2 t_2^n)\\ &= \mathrm{MFT}[f(t_1,t_2)] \end{aligned} \tag{10}$$

Of course, MFT calculations are more time consuming since generally FFT algorithm cannot be used. Depending on the number of time points and desired spectral resolution, calculations can take from few minutes to few hours on a single PC.

### 3.2. Spiral sampling

Spiral sampling of evolution time space determines coordinates of time domain points by the following equations:

$$t_1 = r\cos(ar+\psi) \tag{11a}$$
$$t_2 = r\sin(ar+\psi) \tag{11b}$$

where $r=\sqrt{t_1^2+t_2^2}$ and $a$ is constant (later called "spiral parameter"). Radius value $r$ is incremented with step $\Delta r$ and $\psi$ is the phase of spiral. Point response function of spirally sampled FID can be calculated from the following Fourier Transform integral of signal of zero frequency $f(t_1,t_2)=1$:

$$S(\omega_1,\omega_2)=\int \mathrm{d}t_1\int \mathrm{d}t_2\exp(-\mathrm{i}\omega_1 t_1)\exp(-\mathrm{j}\omega_2 t_2) \tag{12}$$

which, in polar coordinates can be written as

$$\begin{aligned} S(\omega_1,\omega_2) &= \int_0^{2\pi}\mathrm{d}\varphi\int_0^{\infty}\mathrm{d}r\exp[-\mathrm{i}\omega_1 r\cos(ar+\psi)]\\ &\quad \times\exp[-\mathrm{j}\omega_2 r\sin(ar+\psi)]r \end{aligned} \tag{13}$$

where $r$ is a Jacobian included to provide proper integration. Note however, that such procedure is equal to multiplying signal by $r$, which is equivalent of weighting or apodization procedure. It leads to narrowing of spectral lines but makes signal to thermal noise ratio worse in the

case of decaying signals. Often it is preferred to have good $S/N$ ratio than perfectly Lorentzian lineshapes.

Setting polar coordinates for frequency domain, i.e., $R = \sqrt{\omega_1^2 + \omega_2^2}$ and $\Phi = \arctan\left(\frac{\omega_2}{\omega_1}\right)$ followed by integration over $\phi$ results in

$$S(R,\Phi) = 2\pi \int_0^\infty \mathrm{d}r \exp[-\mathrm{i}Rr\cos(\Phi)\cos(ar+\psi)] \times \exp[-\mathrm{j}Rr\sin(\Phi)\sin(ar+\psi)]r \quad (14)$$

For analysis of above expression, Bessel functions of the first kind can be employed. Knowing one of basic properties of Bessel functions:

$$\exp(\mathrm{i}z\cos\theta) = \sum_{n=-\infty}^{\infty} \mathrm{i}^n J_n(z)\cos(n\theta) \quad (15)$$

And trigonometric relations:

$$\cos(\theta)\cos(ar+\psi) = \frac{1}{2}[\cos(\theta - ar - \psi) + \cos(\theta + ar + \psi)] \quad (16a)$$

$$\sin(\theta)\sin(ar+\psi) = \frac{1}{2}[\cos(\theta - ar - \psi) - \cos(\theta + ar + \psi)] \quad (16b)$$

After simple substitution one can obtain expression for integral (Eq. (14)).

$$S(R,\Theta) = 2\pi \int_0^\infty \mathrm{d}r \left[\sum_{n=-\infty}^{\infty} \mathrm{i}^n J_n\left(\frac{Rr}{2}\right)\cos[n(\Theta - ar - \psi)]\right] \times \left[\sum_{n=-\infty}^{\infty} \mathrm{i}^n J_n\left(\frac{Rr}{2}\right)\cos[n(\Theta + ar + \psi)]\right] \times \left[\sum_{n=-\infty}^{\infty} \mathrm{j}^n J_n\left(\frac{Rr}{2}\right)\cos[n(\Theta - ar - \psi)]\right] \times \left[-\sum_{n=-\infty}^{\infty} \mathrm{j}^n J_n\left(\frac{Rr}{2}\right)\cos[n(\Theta + ar + \psi)]\right] r \quad (17)$$

Integrating over $r$ functions of the following formula:

$$J_n\left(\frac{Rr}{2}\right)\cos[n(\Phi + ar + \psi)] \quad (18)$$

gives non-zero results only for spectral coordinates of rings of radii $R = 2na$. Amplitude of each ring is modulated as a function $\cos(n\Phi)$. Phase of spiral ($\psi$) is exactly the phase of this modulation. Resulting lineshapes are shown in Fig. 1.

Positions of artifacts are independent of the maximum value of $r$ and of $\Delta r$. Although, discrete sampling causes periodicity of artifacts. In consequence, it is not possible to set position of the first ring of artifacts as far as desired (as it could be wrongly predicted from equation $R = 2na$).

Using discrete sampling, it is impossible to infinitely increase number of rounds $N$ keeping the same number of points $K$ and $r_{\max}$ (i.e., constant $\Delta r$). In such discrete case Eq. (17) should be rewritten as

$$S(R,\Phi) = 2\pi \sum_{k=0}^{K} \left[\sum_{n=-\infty}^{\infty} \mathrm{i}^n J_n\left(\frac{Rk\Delta r}{2}\right)\cos[n(\Phi - ak\Delta r - \psi)]\right] \times \left[\sum_{n=-\infty}^{\infty} \mathrm{i}^n J_n\left(\frac{Rk\Delta r}{2}\right)\cos[n(\Phi + ak\Delta r + \psi)]\right] \times \left[\sum_{n=-\infty}^{\infty} \mathrm{j}^n J_n\left(\frac{Rk\Delta r}{2}\right)\cos[n(\Phi - ak\Delta r - \psi)]\right] \times \left[-\sum_{n=-\infty}^{\infty} \mathrm{j}^n J_n\left(\frac{Rk\Delta r}{2}\right)\cos[n(\Phi + ak\Delta r + \psi)]\right] k\Delta r \quad (19)$$

Both cosine and Bessel functions are sensitive to discrete sampling and above infinite sum of functions will always contain infinite number of wrongly sampled functions as their frequency $2na$ increases with $n$. But, as long as Nyquist theorem is not fulfilled only for functions of high $n$ (which give non-significant integral) the inner ring is quite free of artifacts. As shown in Fig. 2 increasing parameter $a$ leads to increasing the radius of the first ring of artifacts together with growing number of artifacts inside of it (resulting from integration of growing number of wrongly sampled terms).

### 3.3. Radial sampling as a special case of spiral experiment

Above notation can be used to describe known types of sampling which were presented before, such as radial sampling.

Setting spiral parameter $a = 0$ we obtain sampling scheme for single line radial sampling (Fig. 3a).

This leads to well known relation between time domain sampling pattern and position of artifacts, i.e., artifact ridges are concentrated at:

$$\Phi = \frac{\pi}{2} \mp \psi \quad (20)$$

Typical lineshape from radial sampling processed by MFT is shown in Fig. 3b. It should be noted that result is identical to that obtained from backprojection technique.

### 3.4. Random sampling

In the recent communication [31] we have shown that random off-grid sampling with decaying time domain points density provides superior results in comparison to regular sampling schemes discussed above. This kind of sparse sampling enables collection of data far below the Nyquist condition which has to be fulfilled in the case of conventional regular sampling. Therefore, for random sampling using $n$ points relative data points density $\Theta$ (Eq. (21)) could be set below 1.

$$\Theta = \frac{n \cdot (t_{1\max} \cdot t_{2\max})^{-1}}{\mathrm{SW}_1 \cdot \mathrm{SW}_2} \quad (21)$$

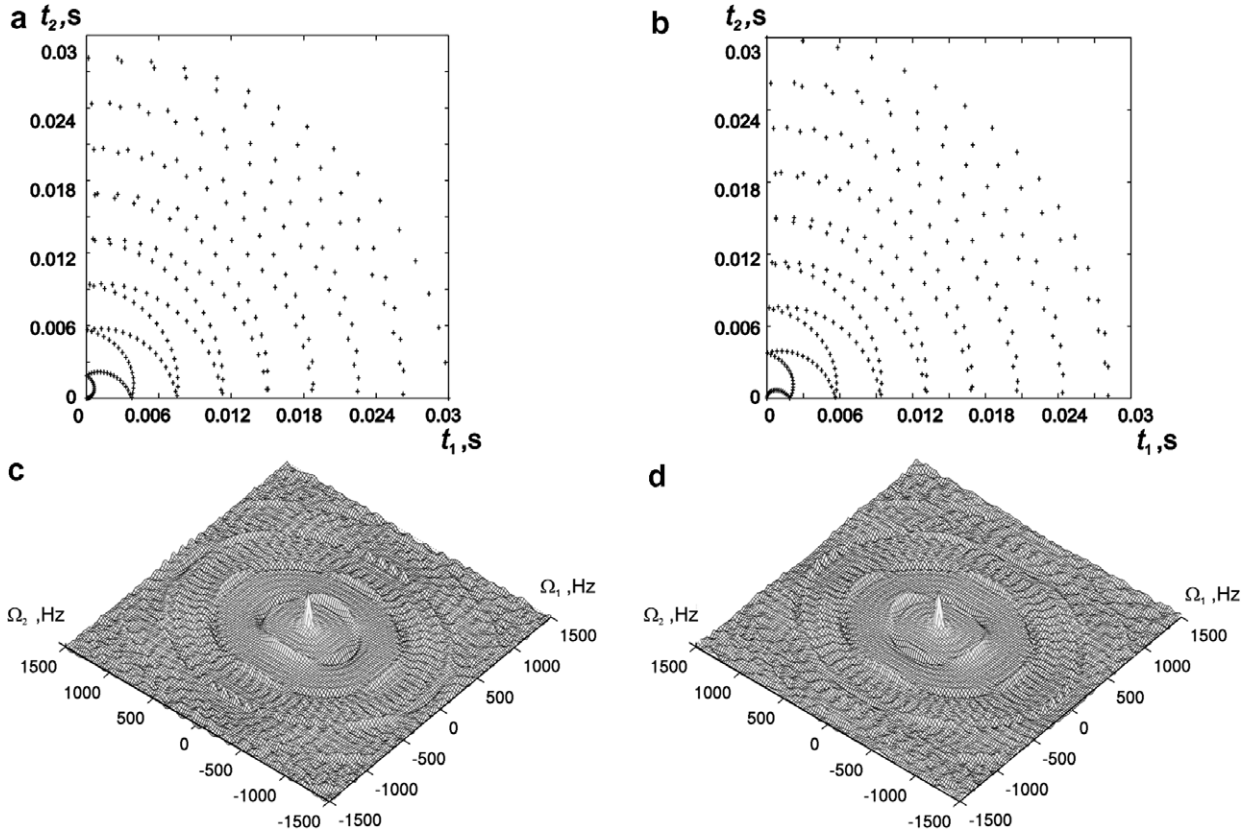


Fig. 1. Comparison of point spread functions (c) and (d) obtained by spiral sampling along two different spiral trajectories, i.e., $(t_1, t_2) = (r|\sin(ar)|, r|\cos(ar)|)$ (a) and $(t_1, t_2) = (r|\cos(ar)|, r|\sin(ar)|)$ (b). Two hundred and fifty-six sampling points were used, spiral parameter $a = 10\pi/256$ and maximum $r$ value $r_{max} = 0.03$ s. The artifact pattern is present in form of rings with modulated amplitude. Phase of modulation can be changed by changing phase $\psi$ of sampling spiral by 90°. In consequence, adding two presented spirals together causes cancelation of the first ring of artifacts [30].

where $t_{1max}$ and $t_{2max}$ are maximum evolution times, $sw_1$ and $sw_2$ are respective spectral widths.

There are two general methods of treating randomly sampled data: weighted samples (WS) method and weighted probability (WP) method [41,42]. The first approach is based on uniform probability density function (PDF) of data points and weighting/apodization prior to FT similarly as in conventional NMR experiments. WP method assumes a non-uniform probability distribution of time domain data points. In the ideal case of oscillatory decaying signal both methods provide identical results, i.e., employing of non-uniform PDF is an equivalent of time domain signal apodization (Fig. 4). However in practice, when decaying signals in the presence of noise are observed, the matched PDF should be chosen [31]. Other important difference in comparison to regular sampling schemes is that the acquisition of point $t_1 = 0$, $t_2 = 0$ is not necessary and should be avoided, as it causes DC offset in frequency domain.

According to sampling theorem [43] time domain signal of finite spectral band is fully specified by its values at equal intervals (limited by Nyquist theorem). Its Discrete Fourier Transform obtained by integration according to rectangular rule (equal weights) is exactly reversible. Equal distance is crucial here. This is no longer possible in the case of non-uniformly sampled signal, even if all sampling points fulfill Nyquist relation and the same method is used for integration with exact weights values (Fig. 5). In other words, the presence of sampling artifacts is associated rather with unequal distances between points than with improper integration. The same integration method gives perfect spectrum from conventional sampling and noisy from random sampling. It is also noteworthy that in fact, in practice weights are set by apodization function which always should be used for truncated signals. Hence, even for conventionally sampled time domain, constant weights for all points are not used which leads to systematic deviation from proper integration.

Although, numerical integration do not allow to obtain spectra free of artifacts from non-conventional data sets, it affects point spread function. Most of numerical integration methods are based on simple polynomial interpolation. In 1D case the maximum allowed degree of polynomial is equal to $n - 1$ (where $n$ is number of recorded time points), but more common are simpler methods: rectangular rule (based on polynomials of zero degree), trapezoidal rule (polynomials of first degree) or more complex Lagrange interpolation [29]. In the case of 2D numerical integration owing to numerical complexity only simplest quadratures could be employed: Delaunay

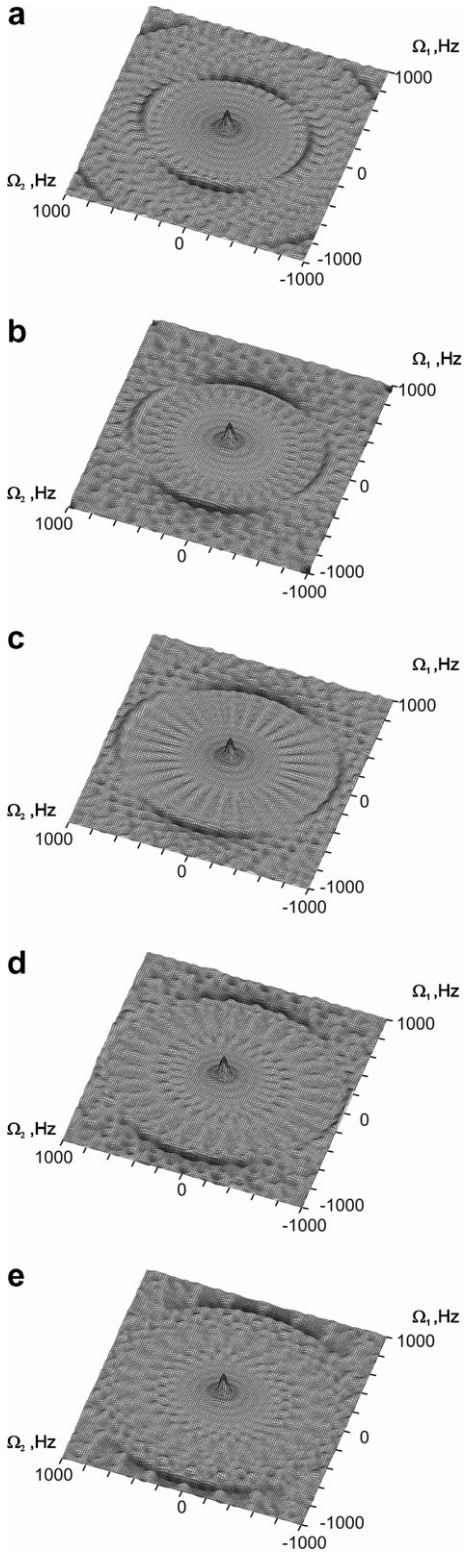


Fig. 2. Comparison of point spread functions versus spiral parameter $a$: (a) $a = 12\pi/256/r_{max}$, (b) $a = 14\pi/256/r_{max}$, (c) $a=16\pi/256/r_{max}$, (d) $a = 18\pi/256/r_{max}$, and (e) $a = 20\pi/256/r_{max}$. All simulations were performed with 256 sampling points, spectral widths of 2000 Hz and $r_{max} = 0.03$ s. With increasing $a$ the radius of first ring of artifacts grows. However, higher order artifacts appear within the ring.

triangulation of time surface [44], which is extension of 1D trapezoidal rule, and Voronoi tessellation [45], which is related to 1D rectangular rule. However, it is known that while polynomial interpolation provides good results in the integration of rational functions it is not well suited for oscillatory functions [46,47].

In the case of non-uniform sampling of time domain, employing rectangular or trapezoidal rule (or its higher dimensional equivalents) could give improved results (in the terms of signal-to-artifact ratio) only in the case of oversampling, i.e., $\Theta > 1$. In our previous work [31] we observed this effect for triangularization of time domain area. Now we discuss similar results obtained using summation over Voronoi cells area. Also in this case increased and frequency dependent artifact pattern is observed. This is due to disregarding of some extremes of oscillatory function between data points, which in case of simple quadratures significantly reduces precision of integration. Since the integrand given in Eq. (4) oscillates with higher frequency far away from the peak position the errors increase with the distance from the signal. This characteristic pattern is observed always, when polynomial approximation of integrand is employed, as shown for example of employing 1D Lagrange interpolation and 2D Voronoi tessellation [36]. The area of the low artifact region in the signal vicinity decreases with decreasing relative points density $\Theta$.

### 3.5. Optimization of random sampling

The random sampling of the evolution time space causes, especially for low relative sampling densities $\Theta$, irregularities in the covering time space. The significant improvement of results and reduction of artifact level could be obtained by the simple modification of random sampling schedule. Instead of random choosing of time coordinates for all points in the limits of maximum evolution time, the time domain is divided into several small cells, each containing one randomly chosen point. For uniform PDF all cells are of equal area, but for non-uniform PDF they are appropriately scaled. This procedure reduces the deviation of distances between time points, but the sampling scheme remains random. The Gaussian distributions of data points using standard and optimized algorithm are compared in Fig. 6. The results of MFT are similar to those obtained using numerical quadratures (i.e., clean area in the signal vicinity is observed), although the signal-to-noise ratio is improved, and the clean region in signal vicinity is significantly larger. This effect is obtained due to more uniform points distribution and therefore better fulfilling of equal weights approximation. The comparison of signal-to-artifact ratio for differently weighted MFT in function of relative data points density $\Theta$ is shown in Fig. 7. The signal-to-artifact ratios were evaluated according to the definition, using root-mean-square of spectral values from the quarter of spectrum opposite to the quarter containing peak.

In Fig. 8, we plot the comparison of spectra obtained using simple summation with weights $w(t_1, t_2) = 1$ (Fig. 8a and b) and with $w(t_1, t_2)$ set to area of Voronoi cells

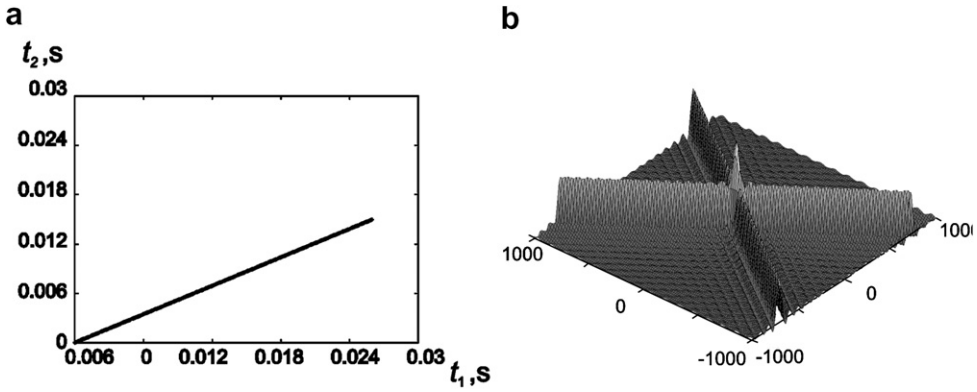


Fig. 3. Single line radial sampling (a) and its point response function after MFT processing (b). Phase $\psi = 30°$ results in ridges at spectral position $\Phi = \pm 60°$. Jacobian $r$ was used during transformation.

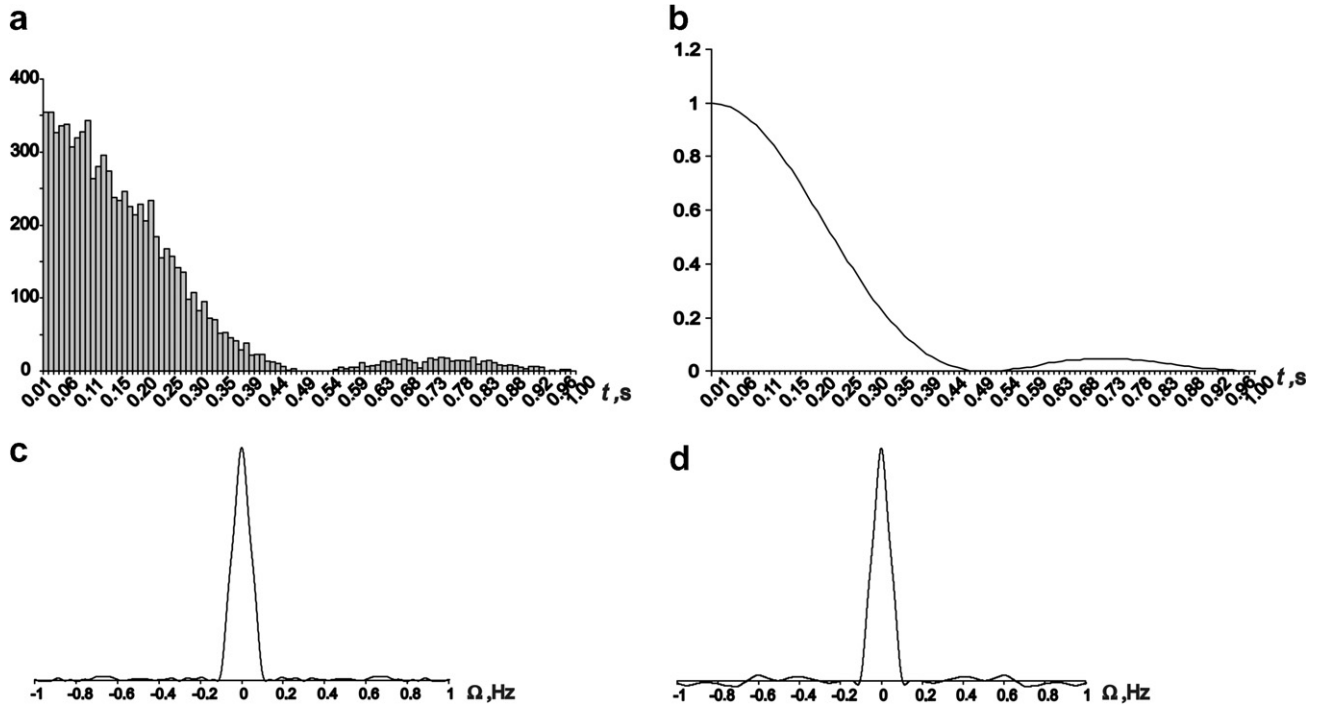


Fig. 4. 1D simulations of weighted samples and weighted probability method using $\left[\frac{\sin(x)}{x}\right]^2$ as PDF (a and c) or weighting function (b and d). (a) Histogram of sampling scheme showing points density, (b) analogical weighting function, (c) Fourier Transform of time domain signal sampled according to scheme (a), and (d) Fourier Transform of randomly distributed, with uniform PDF, data points. Signal of 0 Hz frequency, acquisition time of 1 s and 8192 sampling points was simulated. Lineshape is convolution of Lorentzian function with characteristic triangular function (which is FT of $\left[\frac{\sin(x)}{x}\right]^2$ [43]) in both (c) and (d). Therefore, lineshape resulted from random sampling with non-uniform PDF can be easily predicted, as a convolution of Lorentzian function with Fourier Transform of PDF. In the case of uniform PDF, similarly as for conventional sampling the convolution with weighting profile is observed.

(Fig. 8c and d). The spectra were simulated with very low relative time domain point density $\Theta$ of 2.4%. For spectra shown in Fig. 8a and c the Gaussian data point distribution was used. Whereas, the optimized distribution was employed in the case of spectra plotted in Fig. 8b and d. It is clearly visible that the artifact level is decreased the signal vicinity especially in the case of optimized sampling (Fig. 8a and d). At this relative data points density Voronoi area integration (Fig. 8c and d) increases artifact level, and the ''low noise'' region is very small especially for non-optimized sampling. Similar result was recently reported in the work of Pannetier et al. [36] who showed approx. 15% decreasing of signal-to-artifact ratio in simulated experiments with Voronoi integration and $\Theta$ of 40%. It should be noted, that in real experiment using decaying probability density function, the total noise level (i.e., sum of artifacts and usual thermal noise), in spectra obtained by Voronoi integration would be significantly increased in

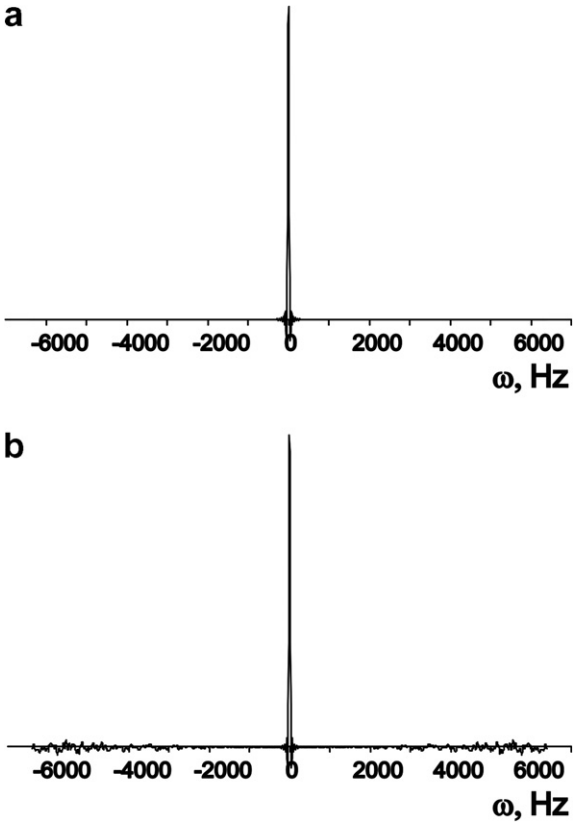


Fig. 5. Numerical evaluation of Fourier integral in the case of regular sampling fulfilling Nyquist theorem (a), and random sampling (uniform PDF) with distance between every neighboring points not exceeding $sw^{-1}$ (b). Both Fourier integrals were calculated using weights equal to distances between points (i.e., rectangular rule). While, the regularly sampled spectrum does not exhibit any artifacts, they are present in the case of random sampling. Thus, presence of sampling artifacts is the matter of sampling scheme rather than integration method.

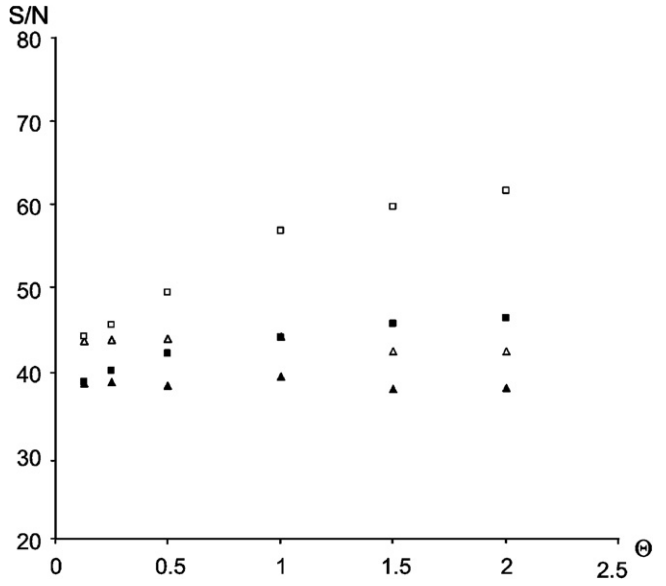


Fig. 7. Signal-to-artifact ratio in 2D simulated spectra. 512 time domain points, $\nu_1 = \nu_2 = 300$ Hz. $t_{1\max} = t_{2\max} = 20$ ms. △, Gaussian distribution with $\sigma = 0.01$ s, MFT using $w(t_1, t_2) = 1$; □, optimized Gaussian distribution with the same $\sigma$, MFT using $w(t_1, t_2) = 1$; ▲, Gaussian distribution with $\sigma = 0.01$ s, MFT using weights set to Voronoi cell areas; ■, optimized Gaussian distribution with the same $\sigma$, MFT using weights set to Voronoi cell areas. The best results are achieved using optimized time domain sampling scheme followed by simple MFT with equal point weights.

comparison to results of MFT with weights $w(t_1, t_2) = 1$. This is due to overweighting of the points for high evolution time.

The non-uniform time domain points distribution causes artifacts which depend on the sampling schedule and signal shape. The relative amplitude of artifacts

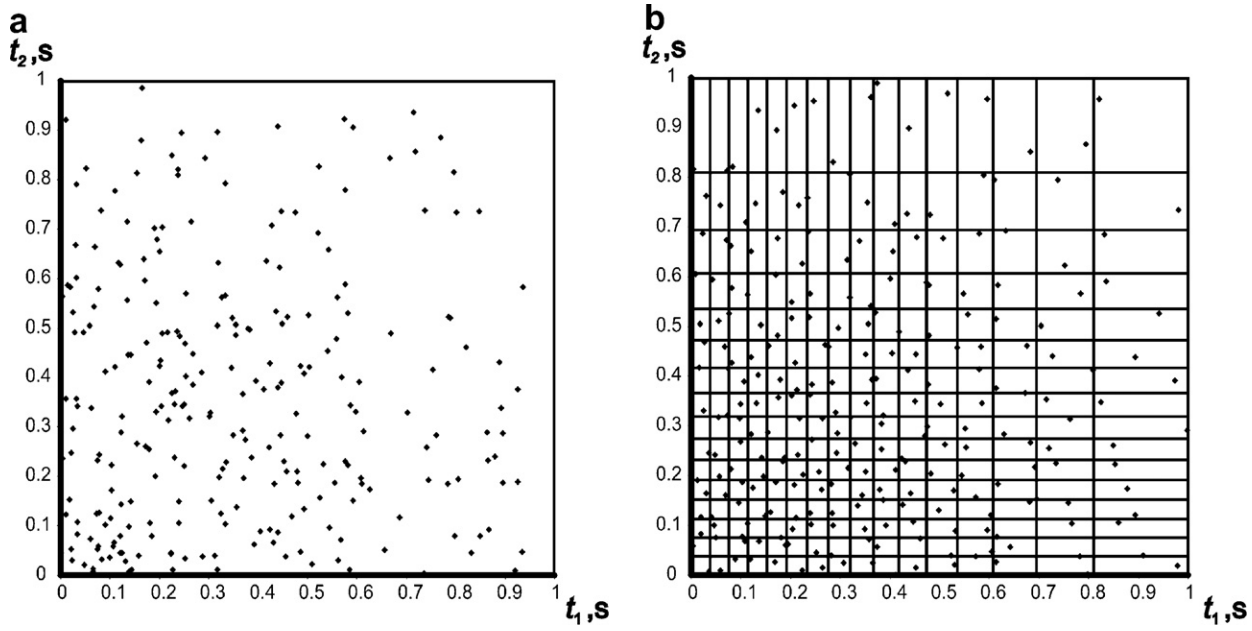


Fig. 6. Illustration of optimized random sampling. (a) Two hundred and fifty-six random points with Gaussian distribution ($\sigma = 0.5$), and (b) the same number of points, according to the same distribution, each placed in the individual cell.

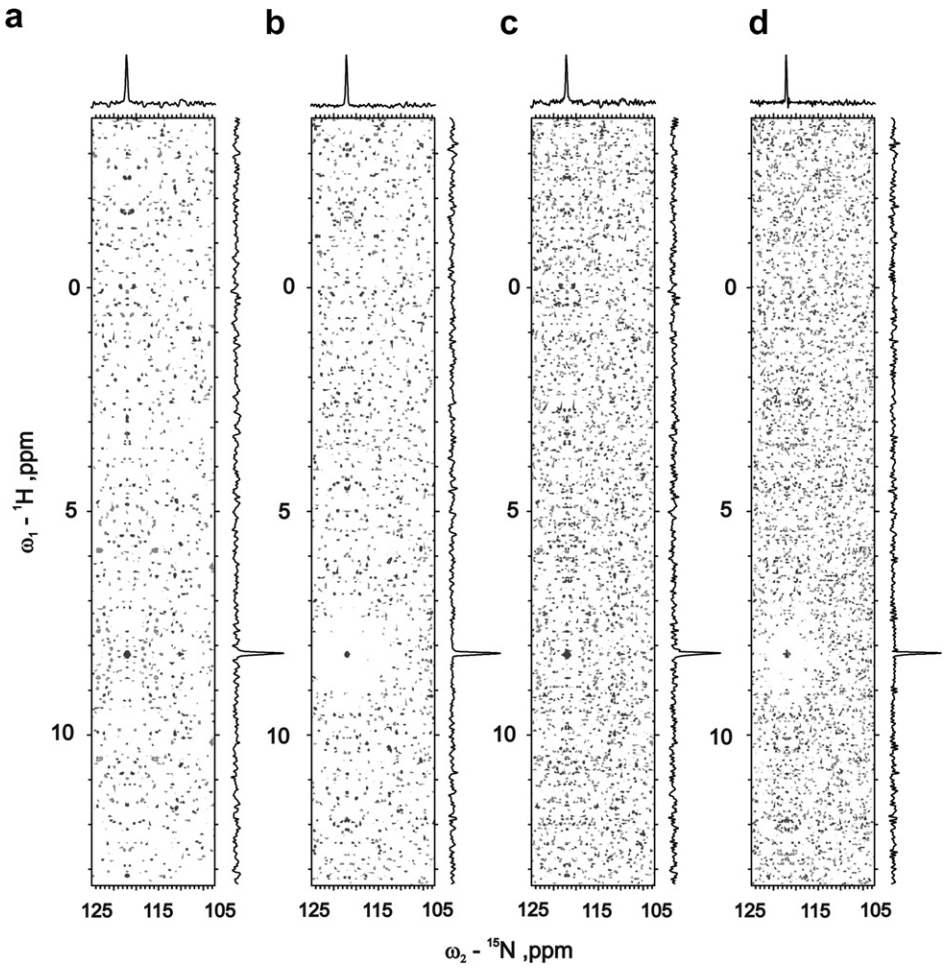


Fig. 8. Comparison of contour plots of 2D spectra obtained by simulation using random time domain points distribution and parameters according to experimental $^{15}$N-edited NOESY-HSQC experiment shown in Fig. 10, but number of time domain points set to 512, which gives points density of 2.4% of Nyquist density. (a and b) Simple summation with weights $w(t_1, t_2) = 1$; (c and d) weights $w(t_1, t_2)$ set to area of Voronoi cells. For spectra (a and c) the Gaussian data point distribution was used, and in the case of (b and d) optimized distribution was employed. Artifact level in spectra (a and b) obtained with constant weights is approximately 15% lower than when Voronoi tessellation was used.

decreases proportionally to the square root of the number of data points. It has been shown in 1D applications (other than NMR), that the correct result could be obtained using all weights equal 1 [41] (assuming equal contributions to the integral given in Eq. (4) from all data points).

To summarize, the proper integration of Eq. (4) improves results of MFT only for the large number of data points, above the Nyquist density. Similarly as it is not possible to avoid signal folding by data processing methods, in the case of conventional regular sampling, it is not possible to obtain ideal spectrum using non-uniform and sparse sampling of the time domain.

### 3.6. Removing artifacts

As mentioned before, shape of artifacts in spectra of non-uniformly sampled signals is determined only by their frequency, amplitude, convolution, and time domain points coordinates used for spectrum acquisition. Hence, artifacts relative position is related to the signal frequency, and their amplitude is proportional to the signal amplitude. Therefore, knowing of time domain points coordinates and frequencies, intensities and linewidths of strong signals it is possible to accurately predict artifact pattern. This allows for selective subtraction of artifacts due to strong peaks. Such procedure is useful in the case of spectra with high dynamic range of signal amplitudes, for example NOESY, where artifacts associated with diagonal peaks may lead to disregarding of weak resonances which are necessary for structural analysis. Cleaning procedure is realized in the following manner (see also flowchart in Fig. 9):

1. Peak-picking of the strongest resonances is performed using standard spectrum visualization software [48]. This can be done automatically. Peaks should be fitted with appropriate function (depending on the time points PDF—Lorentzian or Gaussian) to obtain peak linewidths. List of peaks containing peak frequencies, amplitudes, and linewidths is saved in a file.
2. Cleaning program generates ''artificial'' multidimensional FID as a sum of eight modulation terms needed to obtain quadrature in all three dimensions:

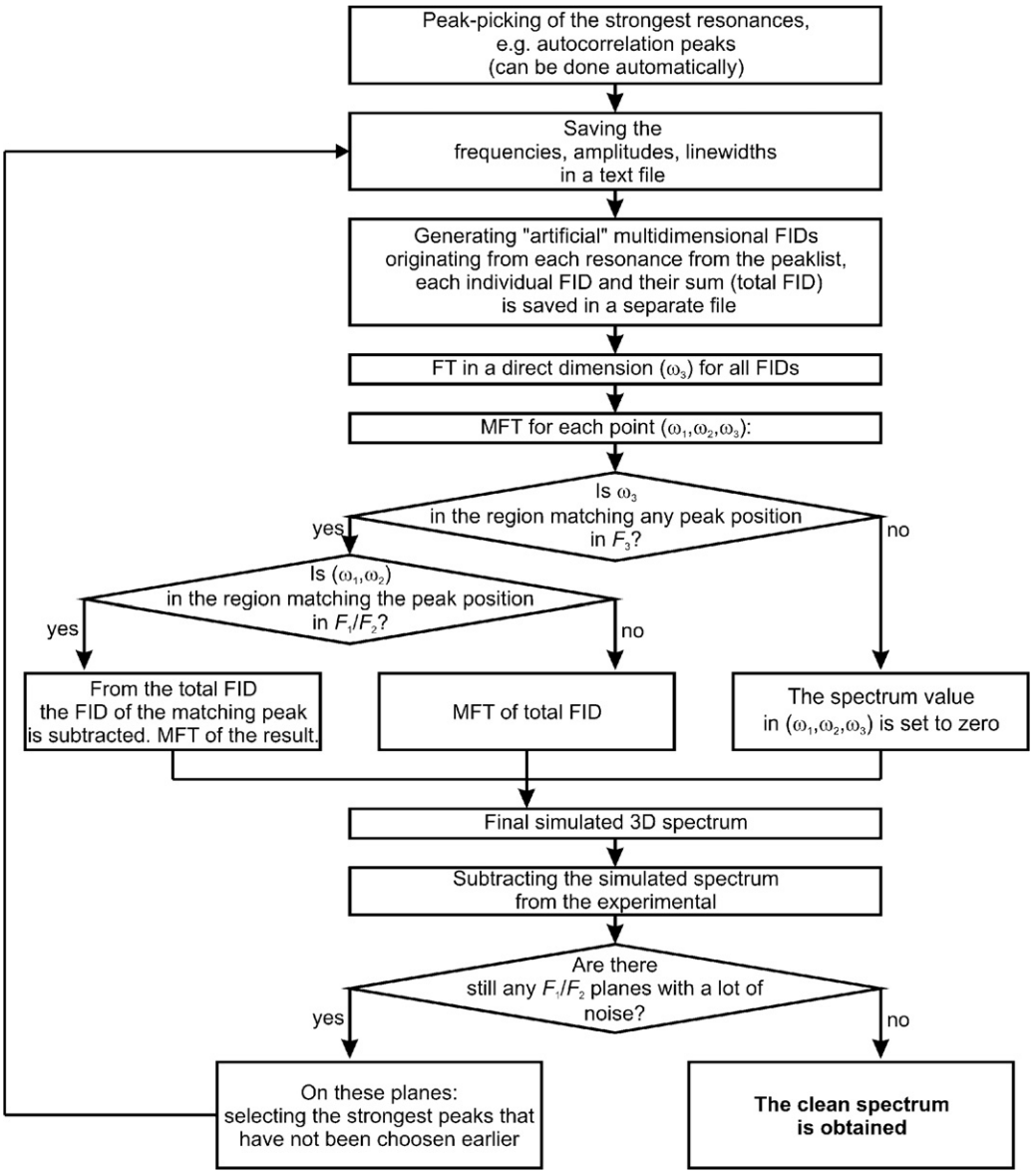


Fig. 9. Flowchart illustrating the idea of cleaning algorithm. It should be noted, that in all experimental examples presented here and tried so far in our lab only one iteration (one peak-picking) had to be performed.

$$\mathrm{FID}(t_1,t_2,t_3)=\sum_i A_i\cos(-\Omega_1^i t_1)\cos(-\Omega_2^i t_2)\cos(-\Omega_3^i t_3)\times\exp(-R_1t_1-R_2t_2-R_3t_3)w(t_1,t_2,t_3)+\cdots \quad (22)$$

where $i$ is the number of peaks and $w(t_1,t_2,t_3)$ are eventual apodization weights. Scaling factors $A_i$ are calculated to obtain correct FID amplitudes from peak intensities and are determined by Fourier Transform at positions of the resonances. Relaxation rates are considered to be equal to peak linewidths. Total FID as well as its $i$ individual components of above sum are saved in separate files.

3. The "artificial" 3D FIDs of all peaks and their sum are transformed in the direct dimension in the same way as a true data and stored separately. Then, the MFT procedure for the total FID is performed in the regions matching with peak positions in $F_3$ (or neighboring to them). For $F_1/F_2$ points in the range of 2.5 linewidth from peak, the FID component of a appropriate frequency is subtracted from the summed FID to avoid deletion of the peaks.
4. Resulting spectrum containing artifact pattern (with no peaks) is subtracted from the experimental spectrum.

It should be noted, that only peak-picking is done by a user and the remaining procedure is performed automatically and does not require adjusting of any parameters.

Similar procedure has been implemented before in 1D FT (or series of 1D FTs), first in astronomy [49], then in NMR for 1D sparse sampling in 2D acquisition [50], removing twisted-peak lineshapes [51] or projection-reconstruction ridges [52]. The difference is that in mentioned

approaches correlation peaks are not omitted during cleaning procedure (as it is not possible in conventional sequential multidimensional FT computed with variable separation) but removed and then reintroduced artificially into final spectrum. Moreover, all these procedures are performed in a large number of iterations, equal to number of removed peaks. In our method, one iteration (using all undoubtedly selected resonances) has given satisfying effects in all experimental cases tried so far. It should be noted that it is much easier to select a large number of strong resonances in one step in the case of random sampling than in Projection Reconstruction, because of lower artifact level.

As an example we present $^{15}$N-edited NOESY. Result of such cleaning procedure is demonstrated in Fig. 10. Removal of artifacts allows finding of new peaks masked by artifacts and does not affect relative signal intensities, thus allowing for estimation of structural constrains. In Fig. 11, we plotted signal intensities in "cleaned" $^{15}$N-edited NOESY spectrum, acquired using random acquisition scheme and processed by MFT, vs. conventional experiment of the same duration. The high correlation coefficient ($R = 0.995$) indicates that both spectra provide the same structural information. Moreover, due to significantly improved resolution, it was possible to find ca. 10% more weak signals in randomly sampled experiment. The computational time in given example was about 3 h.

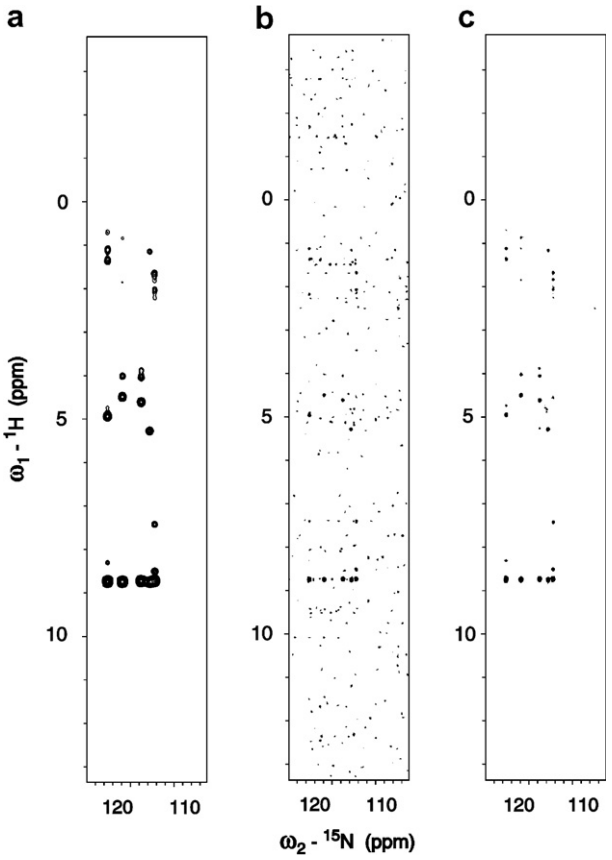


Fig. 10. Comparison of contour plots of $F_1F_2$ planes at $\omega_3(^1\mathrm{H}) = 8.746$ ppm, obtained in $^{15}$N-edited NOESY-HSQC experiment for $^{13}$C, $^{15}$N-labeled ubiquitin on 700 MHz spectrometer, using conventional (a), random sampling (b), and random sampling with artifacts cleaned by simulation and subtraction as described in text (c). The spectral width of $12{,}000 \times 2000 \times 12{,}000$ Hz was set in $F_1$, $F_2$, and $F_3$, respectively. The maximum evolution times $t_1$ and $t_2$ of 30.0 ms, were used in experiment with random sampling, $\Theta = 10.6\%$. In the conventional experiment 115 and 20 $t_1$ and $t_2$ increments, respectively was collected, which is equivalent to maximum evolution times $t_1$ and $t_2$ of 9.6 and 10 ms, respectively. Four scans were coherently added in all four data sets for 2300 $t_1/t_2$ data points, thus the acquisition time of both, conventional and randomly sampled experiments were equal. For conventional spectra cosine weighting function was applied prior to Fourier transformation in all dimensions, while in the case of random sampling with exponential or Gaussian data point distribution only in $t_3$. The spectra were transformed with the resolution of $1024 \times 512 \times 2048$ points in $F_1$, $F_2$, and $F_3$, respectively.

## 4. Experimental

The 3D $^{15}$N-edited NOESY-HSQC spectra were recorded for 1.5 mM $^{13}$C, $^{15}$N double labeled human ubiquitin in 9:1 $H_2O/D_2O$ at pH 4.5 at 298 K on a Varian NMR System 700 spectrometer equipped with a Performa IV z-PFG unit and using the 5 mm $^1$H, $^{13}$C, $^{15}$N—triple resonance probehead with high power $^1$H, $^{13}$C, and $^{15}$N $\pi/2$ pulses of 5.9, 13.5, and 31.0 μs, respectively. The conventional pulse sequence were adapted from the Varian Userlib BioPack package and processed by NMRPipe [53] software saving only amide protons region in $F_3$ dimension. The MFT was performed employing PC with 3.0 GHz Pentium 4 processor running under Linux OS. The software is available from authors. All NMR spectra were analyzed by Sparky [48] program.

## 5. Conclusions

We have shown that Multidimensional Fourier Transform is a simple method to process randomly sampled multidimensional NMR data. Contrary to other approaches it is general and does not require user adjustable parameters and assumptions. This approach enables recording of multidimensional experiments with improved resolution achievable in given acquisition time and retaining all features of conventional spectra. The superior spectral resolution feasible by random sampling and MFT is of high importance regarding biomolecular NMR spectroscopy, and could be also applied for processing of other unconventionally sampled multidimensional signals without necessity of time domain signal interpolation.

The FT processing of non-regularly sampled data always gives rise to artifacts, whose level is lowest in the case of random sampling. In the case of significantly undersampled signals the best results are achieved using equal weights in Fourier integral for all time domain points. On the other hand, described in this communication simple optimization of random sampling schedule improves results owing to better fulfilling of equal weights approximation.

The artifacts level is proportional to signal amplitude, therefore even for highly sensitive cryogenically cooled probes the signal-to-artifact level remains unchanged.

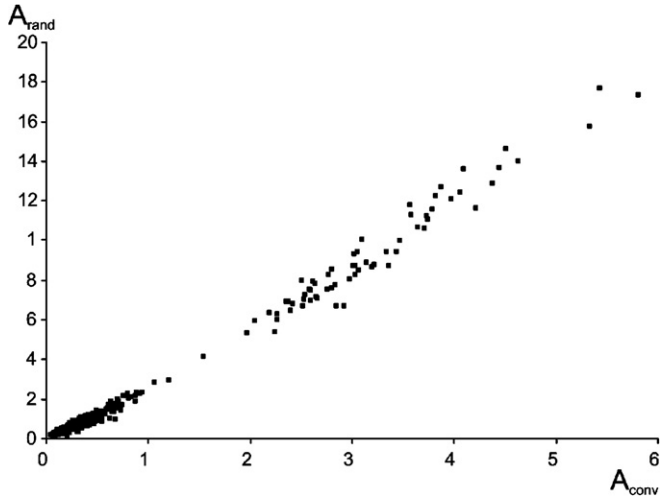


Fig. 11. Correlation between 453 peak intensities (in arbitrary units) in randomly sampled ($A_{rand}$) and conventional ($A_{conv}$), $^{15}$N-edited NOESY-HSQC experiments shown in Fig. 10. The correlation coefficient $R$ of 0.995 was obtained.

However, since the artifacts are exactly predictable on the basis of sampling schedule and signal frequencies it is possible to identify strong signals and subtract calculated artifacts. In the case of spectra with the high dynamic range of signal intensities, as for example NOESY experiments, the removing of artifacts, appearing mainly due to strong diagonal peaks enables to identify additional contacts, and preserves the advantages of high resolution due to sparsely sampled time domain.

## Acknowledgments

This work was supported by Grant Number: N301 07131/2159, founded by Ministry of Science and Higher Education in years 2006–2009. The NMR measurements were accomplished at the Structural Research Laboratory, Chemistry Department, Warsaw University, Poland. The 700 MHz Varian NMR Systems spectrometer was founded by Grant: 217/FNiTP/115/2005 of Foundation of Polish Science and Technology.

## References

[1] J. Jeener, Lecture presented at Ampere International Summer School II, Basko Polje, Yugoslavia, 1971.
[2] G. Bodenhausen, R.R. Ernst, The accordion experiment, a simple approach to three-dimensional NMR spectroscopy, J. Magn. Reson. 45 (1981) 367–373.
[3] G. Bodenhausen, R.R. Ernst, Direct determination of rate constants of slow dynamic processes by two-dimensional "accordion" spectroscopy in nuclear magnetic resonance, J. Am. Chem. Soc. 104 (1982) 1304–1309.
[4] K. Ding, A.M. Gronenborn, Novel 2D triple-resonance NMR experiments for sequential resonance assignments of proteins, J. Magn. Reson. 156 (2002) 262–268.
[5] S. Kim, T. Szyperski, GFT NMR, a new approach to rapidly obtain precise high-dimensional NMR spectral information, J. Am. Chem. Soc. 125 (2003) 1385–1393.
[6] W. Koźmiński, I. Zhukov, Multiple quadrature detection in reduced dimensionality experiments, J. Biomol. NMR 26 (2003) 157–166.
[7] P.C. Lauterbur, Image formation by induced local interactions: examples employing nuclear magnetic resonance, Nature 242 (1973) 190–191.
[8] Ē. Kupče, R. Freeman, New methods for fast multidimensional NMR, J. Biomol. NMR 27 (2003) 101–113.
[9] Ē. Kupče, R. Freeman, Projection-reconstruction of three-dimensional NMR spectra, J. Am. Chem. Soc. 125 (2003) 13958–13959.
[10] R. Freeman, Ē. Kupče, Distant echoes of the accordion: reduced dimensionality, GFT-NMR, and projection-reconstruction of multidimensional spectra, Concept Magn. Res. 23A (2004) 63–75.
[11] Ē. Kupče, R. Freeman, The Radon transform: a new scheme for fast multidimensional NMR, Concept Magn. Res. 22A (2004) 4–11.
[12] B.E. Coggins, R.A. Venters, P. Zhou, Generalized reconstruction of *n*-D NMR spectra from multiple projections: application to the 5-D HACACONH spectrum of protein G B1 domain, J. Am. Chem. Soc. 126 (2004) 1000–1001.
[13] B.E. Coggins, R.A. Venters, P. Zhou, Filtered backprojection for the reconstruction of a high-resolution (4,2)D CH3-NHNOESY spectrum on a 29 kDa protein, J. Am. Chem. Soc. 127 (2005) 11562–11563.
[14] J.W. Yoon, S. Godsill, Ē. Kupče, R. Freeman, Deterministic and statistical methods for reconstructing multidimensional NMR spectra, Magn. Reson. Chem. 44 (2006) 197–209.
[15] D. Malmodin, M. Billeter, Signal identification in NMR spectra with coupled evolution periods, J. Magn. Reson. 176 (2005) 47–53.
[16] D. Malmodin, M. Billeter, Multiway decomposition of NMR spectra with coupled evolution periods, J. Am. Chem. Soc. 127 (2005) 13486–13487.
[17] V. Orekhov, I. Ibraghimov, M. Billeter, Optimizing resolution in multidimensional NMR by three-way decomposition, J. Biomol. NMR 27 (2003) 165–173.
[18] T. Luan, V. Jaravine, A. Yee, C.H. Arrowsmith, V.Y. Orekhov, Optimization of resolution and sensitivity of 4D NOESY using multidimensional decomposition, J. Biomol. NMR 33 (2005) 1–14.
[19] V. Tugarinov, L.E. Kay, I. Ibraghimov, V.Y. Orekhov, High-resolution four-dimensional H-1-C-13 NOE spectroscopy using methyl-TROSY, sparse data acquisition, and multidimensional decomposition, J. Am. Chem. Soc. 127 (2005) 2767–2775.
[20] V.A. Mandelshtam, H.S. Taylor, A.J. Shaka, Application of the filter diagonalization method to one- and two-dimensional NMR spectra, J. Magn. Reson. 133 (1998) 304–312.
[21] G.S. Armstrong, V.A. Mandelshtam, A.J. Shaka, B. Bendiak, Rapid high-resolution four-dimensional NMR spectroscopy using the filter diagonalization method and its advantages for detailed structural elucidation of oligosaccharides, J. Magn. Reson. 173 (2005) 160–168.
[22] E.D. Laue, M.R. Mayger, J. Skilling, J. Staunton, Reconstruction of phase-sensitive two-dimensional NMR spectra by maximum entropy, J. Magn. Reson. 68 (1986) 14–29.
[23] D.P. Frueh, Z.-Y.J. Sun, D.A. Vosburg, C.T. Walsh, J.C. Hoch, G. Wagner, Non-uniformly sampled double-TROSY hNcaNH experiments for NMR sequential assignments of large proteins, J. Am. Chem. Soc. 128 (2006) 5757–5763.
[24] Z.-Y.J. Sun, D.P. Frueh, P. Selenko, J.C. Hoch, G. Wagner, Fast assignment of N-15-HSQC peaks using high-resolution 3D HNcocaNH experiments with non-uniform sampling, J. Biomol. NMR 33 (2005) 43–50.
[25] M.A. Delsuc, D. Tramesel, Application of maximum-entropy processing to NMR multidimensional datasets, partial sampling cas, CR Chim. 9 (2006) 364–373.
[26] D. Rovnyak, D.P. Frueh, M. Sastry, Z.-Y.J. Sun, A.S. Stern, J.C. Hoch, G. Wagner, Accelerated acquisition of high resolution triple-resonance spectra using non-uniform sampling and maximum entropy reconstruction, J. Magn. Reson. 170 (2004) 15–21.
[27] L. Frydman, T. Scherf, A. Lupulescu, The acquisition of multidimensional NMR spectra within a single scan, Proc. Natl. Acad. Sci. USA 99 (2002) 15858–15862.

[28] A. Dutt, V. Rokhlin, Fast Fourier transforms for nonequispaced data. II, Appl. Comp. Harm. Anal. 2 (1995) 85–100.
[29] D. Marion, Fast acquisition of NMR spectra using Fourier transform of non-equispaced data, J. Biomol. NMR 32 (2005) 141–150.
[30] K. Kazimierczuk, W. Koźmiński, I. Zhukov, Two-dimensional Fourier transform of arbitrarily sampled NMR data sets, J. Magn. Reson. 179 (2006) 323–328.
[31] K. Kazimierczuk, A. Zawadzka, W. Koźmiński, I. Zhukov, Random sampling of evolution time space and Fourier transform processing, J. Biomol. NMR 36 (2006) 157–168.
[32] M. Misiak, W. Koźmiński, Three-dimensional NMR spectroscopy of organic molecules by random sampling of evolution time space and multidimensional Fourier transformation, Magn. Reson. Chem. 45 (2007) 171–174.
[33] D. Marion, Processing of ND NMR spectra sampled in polar coordinates: a simple Fourier transform instead of reconstruction, J. Biomol. NMR 36 (2006) 45–54.
[34] B.E. Coggins, P. Zhou, Polar Fourier transforms of radially sampled NMR data, J. Magn. Reson. 182 (2006) 84–95.
[35] B.E. Coggins, P. Zhou, Sampling of the NMR time domain along concentric rings, Magn. Reson. 184 (2007) 207–221.
[36] N. Pannetier, K. Houben, L. Blanchard, D. Marion, Optimized 3D-NMR sampling for resonance assignment of partially unfolded proteins, J. Magn. Reson. 186 (2007) 142–149.
[37] F. Brackx, N. De Schepper, F. Sommen, The Clifford-Fourier Transform, J. Fourier Anal. Appl. 11 (2005) 669–681.
[38] R. da Rocha, J. Vaz Jr., Extended Grassmann and Clifford Algebras, Adv. Appl. Clifford Alg. 16 (2006) 103–125.
[39] R.R. Ernst, J. Bodenhausen, A. Wokaun, Principles of Nuclear Magnetic Resonance in One and Two Dimensions, Oxford Clarendon Press, 1988 (pp. 307–308).
[40] T. Bülow, M. Felsberg, G. Sommer, in: G. Sommer (Ed.), Geometric Computing with Clifford Algebra, Springer-Verlag, Heidelberg, 2001, pp. 187–207.
[41] A. Tarczynski, N. Allay, Spectral analysis of randomly sampled signals: suppression of aliasing and sampler jitter, IEEE Trans. Signal Process. 52 (2004) 3324–3334.
[42] A. Tarczyński, D. Qu, Optimal random sampling for spectrum estimation in DASP applications, Int. J. Appl. Math. Comput. Sci. 15 (2005) 463–469.
[43] R.N. Bracewell, The Fourier Transform and its Applications, McGraw-Hill Higher Education, 2000 (p. 224).
[44] B. Delaunay, Sur la sphère vide, Izvestia Akademii Nauk SSSR, Otdelenie Matematicheskikh i Estestvennykh Nauk 7 (1934) 793–800.
[45] G. Voronoi, Nouvelles applications des paramètres continus à la théorie des formes quadratiques, J. Reine Angew. Math. 133 (1907) 97–178.
[46] E.O. Tuck, A simple "Filon-Trapezoidal" rule, Math. Comput. 21 (1967) 239–241.
[47] G.A. Evans, J.R. Webster, A comparison of some methods for the evaluation of highly oscillatory integrals, J. Comput. Appl. Math. 112 (1999) 55–69.
[48] T.D. Goddard, D.G. Kneller, SPARKY 3, University of California, San Francisco.
[49] J.A. Högbom, Aperture synthesis with a non-regular distribution of interferometer baselines, Astron. Astrophys. Suppl. 15 (1974) 417–426.
[50] J.C.J. Barna, S.M. Tan, E.D. Laue, Use of CLEAN in conjunction with selective data sampling for 2D NMR experiment, J. Magn. Reson. 78 (1988) 327–332.
[51] S.J. Davis, C. Bauer, P.J. Hore, R. Freeman, Resolution enhancement by nonlinear data processing. "HOGWASH" and the Maximum Entropy Method, J. Magn. Reson. 76 (1988) 476–493.
[52] Ē. Kupče, R. Freeman, Fast multidimensional NMR: radial sampling of evolution space, J. Magn. Reson. 173 (2005) 317–321.
[53] F. Delaglio, S. Grzesiek, G.W. Vuister, G. Zhu, J. Pfeifer, A. Bax, A multidimensional spectral processing system based on UNIX pipes, J. Biomol. NMR 6 (1995) 277–293.